Electrochemical, surface analytical and quantum chemical studies on Schiff bases of 4-amino-4H-1, 2, 4-triazole-3,5-dimethanol (ATD) in corrosion protection of aluminium in 1N HNO$_3$

SAM JOHN, K MOHAMMAD ALI and ABRAHAM JOSEPH[*]

Department of Chemistry, University of Calicut, Calicut 673 635, India

Abstract. The present study describes the inhibition of aluminium in 1N HNO$_3$ with different concentrations of 1,2,4-triazole precursors ATD, BATD and DBATD using gravimetric method, potentiodynamic polarization studies (Tafel), electrochemical impedance spectroscopy (EIS), adsorption studies, surface morphological studies and quantum chemical calculations at 298 K. Polarization studies clearly showed that ATD, BATD and DBATD act as mixed type inhibitors. As the electron density around the inhibitor molecule increases due to substitution, the inhibition efficiency also increases correspondingly. Quantum chemical approach was used to calculate some electronic properties of the molecule to ascertain the correlation between inhibitive effect and molecular structure of the inhibitor. The corrosion inhibition efficiencies of these molecules and the global chemical reactivity relate to some parameters, such as E_{HOMO}, E_{LUMO}, gap energy (ΔE), electronegativity (χ), global hardness (η) and the fraction of electrons transferred from the inhibitor molecule to the metallic atom (ΔN). In addition, the local reactivity has been analysed through the Fukui function and condensed softness indices. Both the experimental and theoretical studies agree well in this regard and confirm that DBATD is a better inhibitor than BATD and ATD. The adsorption behaviours of molecules on the copper surface have been studied using molecular dynamics method and density functional theory. The order of inhibitory action is DBATD > BATD > ATD.

Keywords. Aluminium; acid solutions; EIS; polarization.

1. Introduction

Aluminium is an extremely valuable material due to its light weight, high strength, recyclability, corrosion resistance, durability, ductility, formability, and conductivity. Aluminium and its alloys find extensive applications with various industries in different capacities. Aluminium and its alloys, however, are reactive materials and are prone to corrosion. Corrosion of aluminium and its alloys has been a subject of numerous studies due to their high technological value and wide range of industrial applications in aerospace and house hold industries. Though aluminium facilitates the formation of a compact, adherent passive oxide film for its corrosive immunity in various environments, the surface film is amphoteric and dissolves substantially when the metal is exposed to high concentrations of acids or bases (Pourbaix 1966; Khaled and Al-Qahtani 2009). The solubility of the oxide film increases above or below pH 4–9 range and the metal exhibits uniform attack. The use of corrosion inhibitors is inevitable under these circumstances. Most of the efficient acid corrosion inhibitors contain hetero atoms such as N, O, S and multiple bonds in their molecules which activate the process of adsorption. This adsorption process gets activated

as the electron donating efficiency of the inhibitor molecule increases. Most of the hetero atoms in organic molecules bear non-bonding electro pairs in the valence shell and hence possess excellent inhibitory action. The adsorption of molecules on the metal surface is also influenced by their electronic structure, steric factors, aromaticity and p-orbital character of donating electrons (Dessai *et al* 1986; Ajmal *et al* 1994; Abd El-Maksoud 2002).

The aim of the present study is to examine the influence of some selected triazole derivatives on the corrosion inhibition of aluminium in 1N HNO$_3$ solutions using gravimetric, electrochemical techniques, polarization and electrochemical impedance spectroscopy as well as explicit simulations using molecular dynamics and quantum chemical calculations.

## 2. Experimental

2.1 *Inhibitor*

The inhibitor molecule 1, 2, 4-triazole precursor, 4-amino-4H-1, 2, 4-triazole-3, 5-dimethanol (ATD) was synthesized by the condensation of glycolic acid with hydrazine hydrate. Hydrazine monohydrate (E. Merck) (3·75 g, 0·75 mol) was added drop wise at 0°C to 70% aqueous glycolic acid

---

[*]Author for correspondence (drabrahamj@gmail.com)

(E. Merck) (54·3 g, 0·50 mol). The resulting solution was heated at 120°C for 6 h. Then the reflux condenser was replaced with a downward condenser and reaction mixture was heated at 160°C for a further 18 h allowing excess hydrazine and water to distil off. The yellowish crystalline solid formed after cooling was recrystallized from water ATD (Klingele *et al* 2005). (4-(Benzylideneamino)-4H-1, 2, 4-triazole-3,5-diyl) dimethanol (BATD) and (4-(4-(dimethylamino) benzylideneamino))-4H-1,2,4-triazole-3,5-diyl) dimethanol (DBATD) (E. Merck) (1:1 in molar ratio) were prepared by the condensation of ATD with benzaldehyde (E. Merck) (1:1 in molar ratio) and dimethylaminobenzaldehyde (E. Merck) (1:1 in molar ratio), respectively using alcohol as the solvent. The structure of the inhibitor molecules are shown in figures 1a–c.
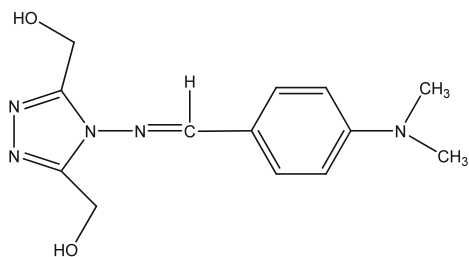
2.2 *Medium*

The medium for the study was made from reagent grade HNO$_3$ (E. Merck) and doubly distilled water. All tests were
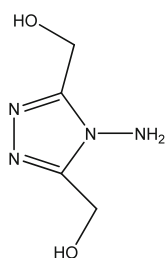
4-amino-4H-1, 2, 4-triazole -3,5-dimethanol(ATD) (a)
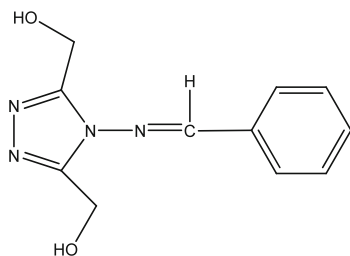
(4-(benzylideneamino)-4H-1, 2, 4-triazole-3, 5-diyl)dimethanol(BATD) (b)

(4-(4-(dimethylamino)benzylideneamino))-4H-1,2,4-triazole-3,5-diyl)dimethanol (DBATD) (c)

Figure 1. Molecular structure of studied triazole derivatives: (**a**) 4-amino-4H-1, 2, 4-triazole-3,5-dimethanol(ATD), (**b**) (4-(benzylideneamino)-4H-1, 2, 4-triazole-3, 5-diyl) dimethanol (BATD) and (**c**) (4-(4-(dimethylamino)benzylideneamino))-4H-1,2,4-triazole-3,5-diyl) dimethanol (DBATD).

performed in aerated medium at room temperature and atmospheric pressure.

2.3 *Materials*

The working electrode was of 100% pure aluminium as determined by EDX spectra. The metal specimens used in weight loss studies are cut into $4·8 \times 1·9$ cm^2 coupons. For electrochemical studies, same type of coupons was used but only 1 cm^2 area was exposed during each measurements. Before measurements the samples were polished using different grades of emery paper followed by washing with ethanol and acetone.

2.4 *Weight loss measurements*

The weight loss experiments were carried out under total immersion conditions in test solution maintained at 300 K. Metal specimens were cleaned according to ASTM standard G-1-72 procedure (Ailor 1971; Talati and Modi 1975; Bag *et al* 1993; McCafferty *et al* 1999). The experiments were carried out in a beaker containing 250 ml solution. After the exposure period the specimens were removed, washed initially under running tap water, to remove the loosely adhering corrosion products and finally cleaned with 70% HNO$_3$ for 3 min followed by acetone. Experiments were conducted at the same temperature with different inhibitor concentrations to find out the optimum inhibitor concentration that shows maximum inhibitive efficiency. From the weight loss in each experiment the corrosion rate was calculated in milli meter/year (mm/yr). In each case, duplicate experiments were conducted which showed that the results obtained were within ± 1% of the first. Whenever variations were very large, the data were confirmed by a third test. The percentage inhibitive efficiency was calculated using the relation

$$\%IE = \frac{W_0 - W}{W_0} \times 100, \tag{1}$$

where W_0 and W are the weight losses in the uninhibited and inhibited solutions, respectively.

2.5 *Electrochemical measurements*

Electrochemical tests were carried out in a three-electrode corrosion cell with platinum sheet (1 cm^2 surface area) as auxiliary electrode and saturated calomel electrode (SCE) as the reference electrode. The working electrode was first immersed in the test solution and after attaining a steady state open circuit potential (OCP), electrochemical measurements were carried out with a Gill AC computer controlled electrochemical workstation (ACM, UK, model no: 1475). Electrochemical impedance spectroscopy (EIS) measurements were carried out with an amplitude of 10 mV (RMS) AC sine wave in a frequency range of 10 kHz to 1 Hz. The potentiodynamic

polarization curves were obtained in the potential range of -250 mV to $+250$ mV with a sweep rate of 16 mV/s.

2.6 *Computational study*

Complete geometry optimization of the metal specimen are performed using the density functional theory (DFT) with Beck's three parameter exchange functional along with Lee-Yang-Parr non-local correlation functional (B3LYP) with 6–31G* basis set implemented in Gaussian 03 program package (Frisch *et al* 2003; Ebenso *et al* 2010). Frontier molecular orbitals (HOMO and LUMO) may be used to interpret the adsorption characteristics of inhibitor molecules on the metal surface.

The local reactivity of the inhibitor molecules was analysed through an evaluation of the Fukui indices (Arslan *et al* 2009). Fukui indices are a measurement of the chemical reactivity, as well as an indicator of the reactive regions and the nucleophilic and electrophilic behaviours of the molecule. The regions of a molecule where the Fukui function is large are chemically softer than the regions where the Fukui function is small, and by invoking HSAB principle in a local sense, one may establish the behaviour of different sites with respect to hard or soft reagents. The Fukui function $f(\vec{r})$ is defined as the derivative of the electronic density, $\rho(\vec{r})$, with respect to the number of electrons, N, at a constant external potential, $\sigma(\vec{r})$

$$f(\vec{r}) = \left(\frac{\partial \rho(\vec{r})}{\partial N}\right)_{\sigma(\vec{r})}. \tag{2}$$

If the effects of relaxation associated with the addition or removal of electronic charges are not considered, then

$$\rho^{+}(\vec{r}) \approx \rho_{\text{LUMO}}(\vec{r}), \tag{3}$$

$$\rho^{-}(\vec{r}) \approx \rho_{\text{HOMO}}(\vec{r}), \tag{4}$$

where $\rho_{\text{LUMO}}(\vec{r})$ is the density of the lowest unoccupied molecular orbital and $\rho_{\text{HOMO}}(\vec{r})$ the density of the highest occupied molecular orbital (Yang and Mortier 1986; Gece 2008; Solmaz *et al* 2008). The condensed Fukui functions are found by taking the finite difference approximations from Mulliken population analysis of atoms in triazole derivatives, depending on the direction of the electron transfer

$$f_k^{+} = q_k(N+1) - q_k(N), \tag{5}$$

$$f_k^{-} = q_k(N) - q_k(N-1), \tag{6}$$

where q_k is the gross charge of atom, k, in the molecule i.e. the electron density at a point r in space around the molecule. N corresponds to the number of electrons in the neutral molecule, $N+1$ corresponds to an anion, with an electron added to the LUMO of the neutral molecule and

$N-1$ represents the cation with an electron removed from HOMO of the neutral molecule. All calculations are done at the ground-state geometry. These functions can be condensed to the nuclei by using an atomic charge partitioning scheme, such as Mulliken population analysis in (3)–(6). An easy graphical display technique was also used based on the Fukui functions. Instead of calculating the molecular orbitals for the neutral, cation, and anion, we can just add or subtract electrons from the molecular orbitals of the neutral molecule. Though this procedure is not as good as the first method, it does give a quick graphical display of the susceptibility to different kinds of attack.

The molecular dynamics (MD) simulation was performed using Material Studio 4·3 software from Accelrys Inc. Al(110) plane was chosen for the simulation study. The interaction energy, $E_{\text{interaction}}$, between the aluminium surface and the inhibitor molecule was calculated as

$$E_{\text{interaction}} = E_{\text{total}} - (E_{\text{surface}} + E_{\text{inhibitor}}), \tag{7}$$

where E_{total} is the total energy of Al-metal and inhibitor molecules. E_{surface} and $E_{\text{inhibitor}}$ are the energy of aluminium and inhibitor molecules, respectively. The binding energy of the inhibitor molecule is the negative value of the interaction energy

$$E_{\text{binding}} = -E_{\text{interaction}}.$$

2.7 *Scanning electron microscopy (SEM)*

The study of the surface morphology of the metal specimen in both absence and presence of inhibitor molecules were carried out by using a Digital Microscope Imaging Scanning Electron Microscope model SU6600 (Serial No: HI-2102–0003) with an accelerating voltage of 20 kV, at a scan speed=slow 5 and calibration scan speed=25. Samples were attached on the top of an aluminium stopper by means of a carbon conductive adhesive tape. All micrographs of the specimen were taken at a magnification of 500×.

3. Results and discussion

3.1 *Weight loss measurements*

Weight loss studies were performed at various time intervals in the absence and presence of different concentrations (10–200 ppm) of ATD, BATD and DBATD. The increase in the inhibitor concentration was accompanied by a decrease in weight loss and corrosion rate and an increase in percentage inhibition efficiency (data not included in the text). These data lead to the conclusion that ATD, BATD and DBATD act as inhibitors for aluminium in 1N HNO$_3$ solution.

3.2 *Potentiodynamic polarization measurements*

Figure 2 shows anodic and cathodic polarization curves of aluminium in 1N HNO$_3$ solution, without and with inhibitor molecules at room temperature (25 $\pm$ 1°C) after immersion for 1 h. It is observed that both cathodic and anodic curves show lower current density in presence of the inhibitor molecules. This indicates that triazole precursors inhibit the corrosion process. The polarization measurements also clearly illustrate the fact that the inhibitor molecules under the studied conditions, brings down the corrosion current without causing any considerable change in the corrosion mechanism, suggesting that the inhibitors show mixed type behaviour. According to corrosion theory (Jones 1983), the rightward shift of the cathodic curves reveal that corrosion is mainly accelerated by cathode reactions. Additionally, the potentiodynamic polarization curves in figure 2 exhibit no steep slope in the anodic range, meaning that no passive films are formed on the aluminium surface. The shape of the graphs remain the same for these three different inhibitors and therefore, only the representative graphs are given in the text. Consequently, aluminium may directly dissolve in 1N HNO$_3$ solutions. The electrochemical reactions for aluminium in HNO$_3$ solution (McCafferty 2005; Khaled *et al* 2009; Zhang and Hua 2010) may be described as follows
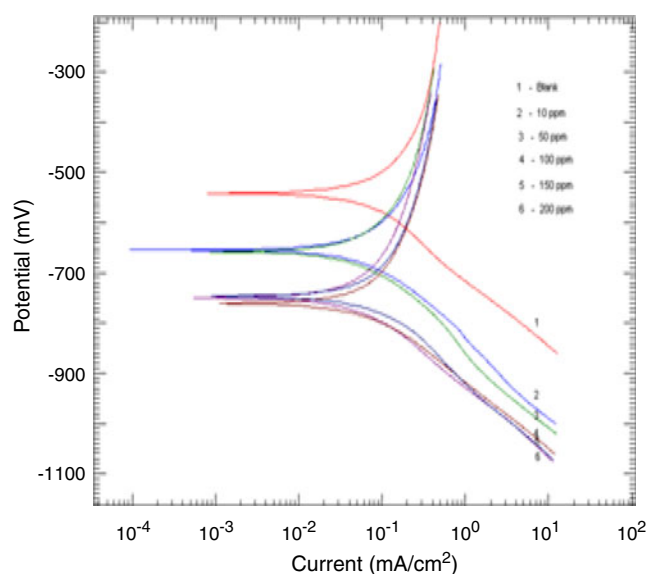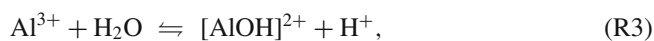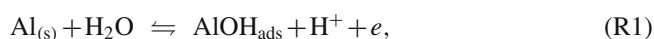
$$Al_{(s)} + H_2O \rightleftharpoons AlOH_{ads} + H^+ + e, \qquad (R1)$$

$$AlOH_{ads} + H_2O + H^+ \rightleftharpoons Al^{3+} + 6H_2O + 2e, \qquad (R2)$$

$$Al^{3+} + H_2O \rightleftharpoons [AlOH]^{2+} + H^+, \qquad (R3)$$

$$[AlOH]^{2+} + X^- \rightleftharpoons [AlOHX]^+. \qquad (R4)$$

Figure 2. Anodic and cathodic tafel lines for aluminium in 1N HNO$_3$ with different concentrations of ATD inhibitors.

The controlling step in the metal dissolution is the complexation reaction between hydrated cation and anion X$^-$ (R4).

Figure 2 shows that with increasing concentrations of inhibitor molecules, the corrosion current density (i_{corr}) decreased considerably. The maximum decrease in the corrosion current density was observed for DBATD. Inspection of polarization curves in figure 2 shows that it was not possible to evaluate the cathodic Tafel slope as there is no visible linear region that prevents linear extrapolation to E_{corr} of the cathodic polarization curves. It has been shown that in the Tafel extrapolation method, use of both the anodic and cathodic Tafel regions is undoubtedly preferred over the use of only one Tafel region (Quartarone *et al* 2008). However, the corrosion rate can also be determined by Tafel extrapolation of either the cathodic or anodic polarization curve alone. If only one polarization curve is used, it is generally the cathodic curve which usually produces a longer and better defined Tafel region. Anodic polarization may sometimes produce concentration effects, due to passivation and dissolution, as noted above, as well as roughening of the surface which can lead to deviations from Tafel behaviour. The situation is quite different here; the anodic dissolution of aluminium in aerated 1N HNO$_3$ solution obeys Tafel's law. The anodic curve is, therefore, preferred over the cathodic one for the Tafel extrapolation method. However, the cathodic polarization curve displays a limiting diffusion current due to the reduction of dissolved oxygen. Thus, the cathodic process is controlled by concentration polarization rather than activation polarization, which prevented linear extrapolation of the cathodic curves. Similar results were reported earlier also (Chetouani *et al* 2005; Amin and Khaled 2010; Labjar *et al* 2010). The values of electrochemical kinetic parameter, corrosion potential (E_{corr}), corrosion current density (i_{corr}) and Tafel slopes (β_a and β_c) are determined from these experiments by extrapolation method and listed in table 1. The corrosion inhibition efficiency was calculated using the relation

$$\%IE = \frac{I_{corr*} - I_{corr}}{I_{corr*}} \times 100, \qquad (8)$$

where I_{corr*} and I_{corr} are uninhibited and inhibited corrosion current densities, respectively determined by extrapolation of Tafel lines in the corrosion potential. The inhibitor molecules first adsorb on the metal surface by blocking the available reaction sites (Amin *et al* 2007). The surface coverage increases with the inhibitor concentration. The presence of defects on the metal surface permits free access to H$^+$ ions (Ashassi-Sorkhabi *et al* 2006) and a significant dissolution of metal takes place, followed by desorption of the surface film from the metal surface (Tsuru *et al* 1978). The formation of inhibitor film on the metal surface provides considerable protection to aluminium in acid environment. This film reduces the active surface area exposed to the corrosive medium and delays the hydrogen evolution and metal dissolution.

Table 1. Polarization parameter and inhibition efficiency for corrosion of aluminium in 1N HNO₃ solutions in absence and presence of different concentrations of inhibitors at room temperature.

| Inhibitor type	Conc. (ppm)	E_{corr}(mV(SCE))	β_a(mV dec^{-1})	β_C(mV dec^{-1})	i_{corr}(μA cm^{-2})	$\eta(\%)$	C.R. (mm/yr)
Blank		−632	347	167	0·1314	—	1·4304
	10	−601	287	167	0·1101	16·21	1·1209
	50	−542	245	166	0·0794	39·57	0·8650
ATD	100	−760	227	137	0·0603	54·11	0·6568
	150	−748	198	113	0·0526	59·96	0·5731
	200	−756	160	99	0·0500	61·94	0·5456
	10	−675	283	164	0·0797	39·34	0·8682
	50	−741	273	144	0·0732	44·29	0·7984
BATD	100	−737	196	136	0·0484	63·16	0·5278
	150	−648	99	77	0·0465	64·61	0·5071
	200	−743	91	63	0·0249	81·05	0·2717
	10	−681	281	167	0·0761	42·05	0·8524
	50	−700	270	151	0·0714	45·66	0·7714
DBATD	100	−717	185	144	0·0471	64·23	0·5173
	150	−691	136	109	0·0437	66·74	0·4870
	200	−692	103	99	0·0214	83·17	0·2616

3.3 *Electrochemical impedance spectroscopy (EIS)*

Nyquist and Bode plots of ATD, BATD and DBATD in 1N HNO₃ solution in the absence and presence of various concentrations of triazole derivatives are given in figures 3 and 4. The shape of the graphs (Nyquist and Bode) remain the same for these three different inhibitors and therefore, only the representative graphs are given in the text. The impedance spectra show a single semicircle and the diameter of the semicircle increases with increasing inhibitor concentrations. These diagrams indicate that the impedance spectra consist of one capacitive loop at high frequency and the high frequency capacitive loop was attributed to charge transfer of the corrosion process (Bentiss *et al* 2000). Various parameters such as charge-transfer resistance (R_{ct}), double layer capacitance (C_{dl}) and i_{corr} were obtained from impedance measurements and the results are given in table 2. R_{ct} values were calculated from the difference in impedance at lower and higher frequencies as suggested by Tsuru *et al* (1978). C_{dl} values were calculated from the frequency at which the imaginary component of impedance was maximum (Z_{max}) using the reaction

$$C_{dl} = \frac{1}{2\pi f_{max}}\frac{1}{R_{ct}},$$

where f_{max} is the frequency at which the imaginary component of impedance is maximum. The inhibition efficiency got from the charge-transfer resistance is calculated by the following relation:

$$IE\% = \frac{R_{ct} - R_{ct}^*}{R_{ct}} \times 100, \tag{9}$$
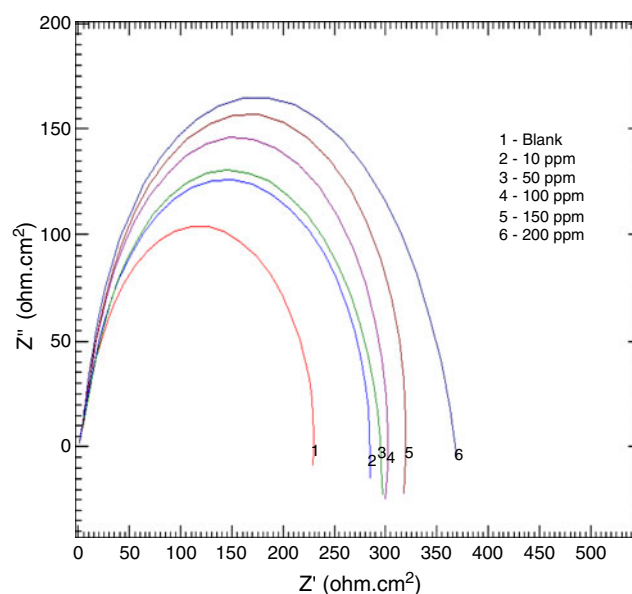
Figure 3. Nyquist diagrams for aluminium in 1N HNO₃ containing different concentrations of ATD.

where R_{ct} and R_{ct}^* represent the resistance of charge transfer in the presence and absence of inhibitors, respectively. R_{ct} corresponds to the diameter of the loop and the R_{ct} values of ATD, BATD and DBATD increases with increasing inhibitor concentration whereas C_{dl} values show opposite trend. These observations support the fact that the corrosion of aluminium in 1 N HNO₃ is controlled by a charge transfer process. The decrease in C_{dl} is due to the gradual replacement of water molecules by the adsorption of the organic molecules at metal/solution interface, leading to a protective film on the metal (Wang *et al* 2007).

3.4 *Quantum chemical calculations*

The energy of the highest occupied molecular orbital (HOMO), is a measure of electron donating ability of a molecule and explains the adsorption characteristics on metallic surface. A high E_{HOMO} value expresses intrinsic electron donating tendency to an appropriate acceptor, i.e. any molecule with lower HOMO energy and empty molecular orbital, while, E_{LUMO}, the energy of the lowest unoccupied molecular orbital signifies the electron receiving
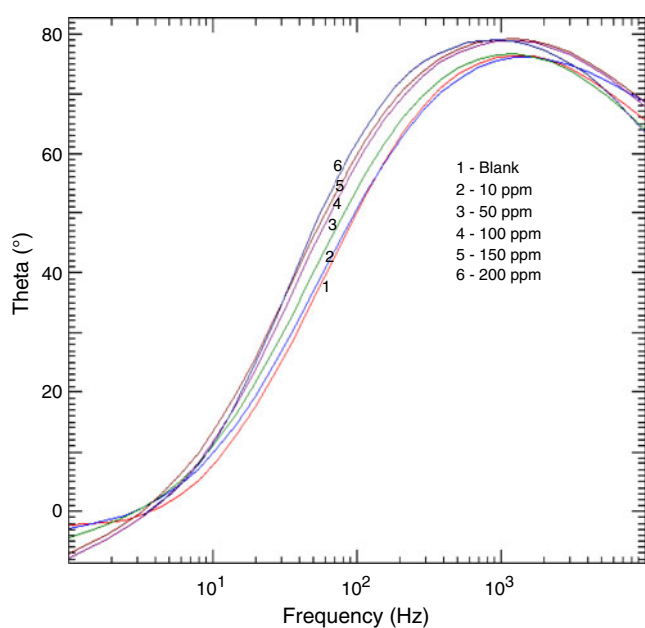

Figure 4. Bode diagrams for aluminium in 1N HNO$_3$ containing different concentrations of ATD.

tendency of a molecule. Accordingly, the difference between LUMO and HOMO energy levels, the dipole moment (μ), the electron charge on hetero-atoms and the total energy of inhibitor molecules were determined. Based on these, the calculated difference ($E_{LUMO} - E_{HOMO}$) demonstrates inherent electron donating ability and measures the interaction of the inhibitor molecule with the aluminium surface. All these computational calculations have been performed in the gas phase. The highest occupied molecular orbital (HOMO) and the lowest unoccupied molecular orbitals (LUMO) are shown in figures 5 and 6. According to the frontier molecular orbital theory of chemical reactivity, transition of electron is due to an interaction between the highest occupied molecular orbital and lowest unoccupied molecular orbital (LUMO) of reacting species. The energy of HOMO is directly related to the ionization potential and characterizes the susceptibility of the molecule toward attack by electrophiles. The energy of LUMO is directly related to the electron affinity and characterizes the susceptibility of the molecule toward attack by nucleophiles. The higher value of E_{HOMO} and lower value of the gap energy, ΔE, show that DBATD acts as a better inhibitor than BATD and ATD. The calculated values of the ionization potential (I) and the electron affinity (A) by the application of Koopmans' theorem are shown in table 3. According to the Hartree–Fock theorem, a relationship exists between the energies of HOMO, LUMO, ionization potential and electron affinity as $-E_{HOMO} = I$; $-E_{LUMO} = A$. Although no formal proof of this theorem exists within DFT, its validity is generally accepted. For χ and η, their operational and approximate definitions are

$$-\mu = (I+A)/2 = \chi, \ \eta = (I-A)/2.$$

Two systems, Al and inhibitor, are brought together, electrons will flow from lower χ (inhibitor) to higher χ (Al),

Table 2. Impedance parameter and inhibition efficiency for corrosion of aluminium in 1N HNO$_3$ solutions in absence and presence of different concentrations of inhibitors at room temperature.

Inhibitor	Conc. (ppm)	$R_{ct}(\Omega\ cm^2)$	$C_{dl}(\mu F\ cm^{-2})$	$i_{corr}(\mu A\ cm^2)$	C.R. (mm/yr)	n	$\eta(\%)$
Blank		225	12·61	0·1158	1·262	0·96	—
	10	281	12·41	0·0926	1·0088	0·94	20·06
	50	293	12·32	0·089	0·9696	0·94	23·2
ATD	100	299	10·89	0·0872	0·9501	0·98	24·72
	150	316	10·7	0·0825	0·8987	0·97	28·8
	200	369	10·69	0·0757	0·7707	0·92	38·93
	10	286	12·36	0·086	0·9981	0·95	21·26
	50	297	11·22	0·0814	0·9491	0·96	24·25
BATD	100	307	10·67	0·0772	0·9272	0·96	26·54
	150	339	10·54	0·0735	0·8767	0·97	33·66
	200	382	10·31	0·0718	0·7522	0·93	41·08
	10	286	12·1	0·0817	0·9765	0·97	21·21
	50	299	11·05	0·0794	0·9507	0·97	24·74
DBATD	100	316	10·17	0·0744	0·9171	0·98	28·83
	150	342	9·87	0·0728	0·8653	0·95	34·12
	200	395	9·56	0·0702	0·7187	0·94	43·04

until the chemical potentials become equal. As a first approximation, the fraction of electrons transferred (Sastri and Perumareddi 1997), ΔN, will be given by

$$\Delta N = \frac{\chi_{Al} - \chi_{inhi}}{2\left(\eta_{Al} + \eta_{inhi}\right)}, \qquad (10)$$

where Al is the Lewis acid according to HSAB concept (Pearson 1963, 1998). The difference in electronegativity drives the electron transfer, and the sum of hardness parameters acts as resistance (Do 1980). In order to calculate the fraction of electrons transferred, a theoretical value for the electronegativity of bulk aluminium was used, $\chi_{Al} \approx 3.23$ eV, and a global hardness of $\eta_{Al} \approx 0$, by assuming that for a metallic bulk $I = A$ because they are softer than the neutral metallic atoms. From table 3, it is evident that the fraction of electrons transferred, ΔN, is high for DBATD and hence it shows higher inhibition efficiency.

The local reactivity is analysed by means of the condensed Fukui function. The condensed Fukui functions allow us to distinguish each part of the molecule on the basis of its distinct chemical behaviour due to different functional groups or substituents. Thus, the site for nucleophilic attack will be the place where the value of f_k^+ is a maximum and the site for electrophilic attack will be the place where the value of f_k^- is maximum. The values of the Fukui functions for a nucleophilic and electrophilic attack are given for the three inhibitors in table 4 (only for the nitrogen, oxygen and carbon atoms). Inspection of the values of Fukui functions presented in table 4 shows that DBATD has propitious zones for nucleophilic attack located on N16, C17, C20, C22, and N29 while BATD has only on C1, C2, N4 and N5. ATD has only nucleophilic centres on N3 and N4. Data in table 4 shows that DBATD has more susceptible sites for adsorption on the aluminium surface, which reflects its highest inhibition performance. The HOMO location on each system agrees with the atoms that exhibit greatest values of indices of Fukui, both indicate the zones by which the molecule would be adsorbed on the mild surface.

3.5 *Adsorption isotherm*

The nature of interaction between the inhibitor molecules and metal surface can be obtained from the adsorption isotherms.
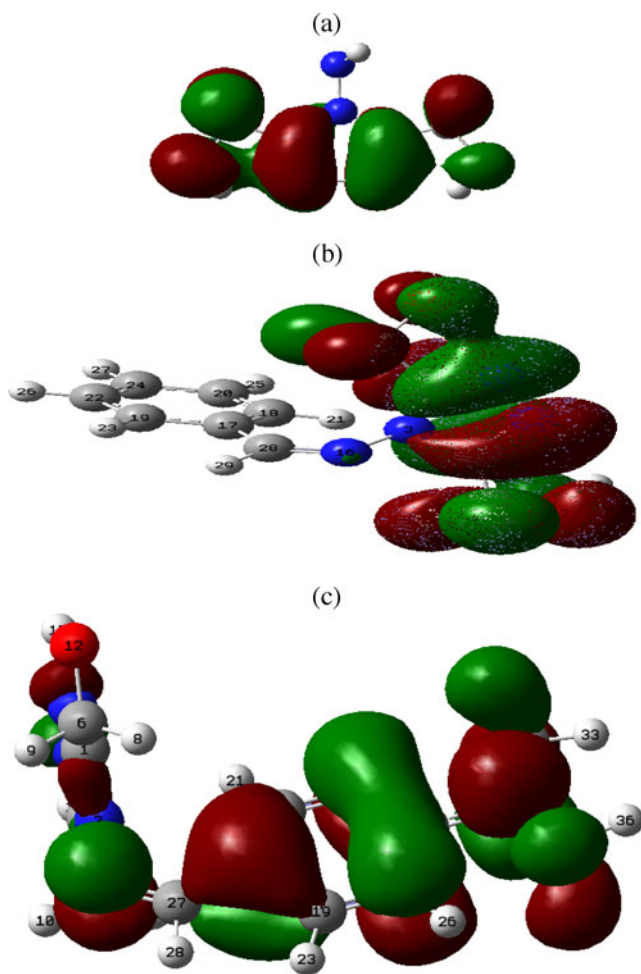

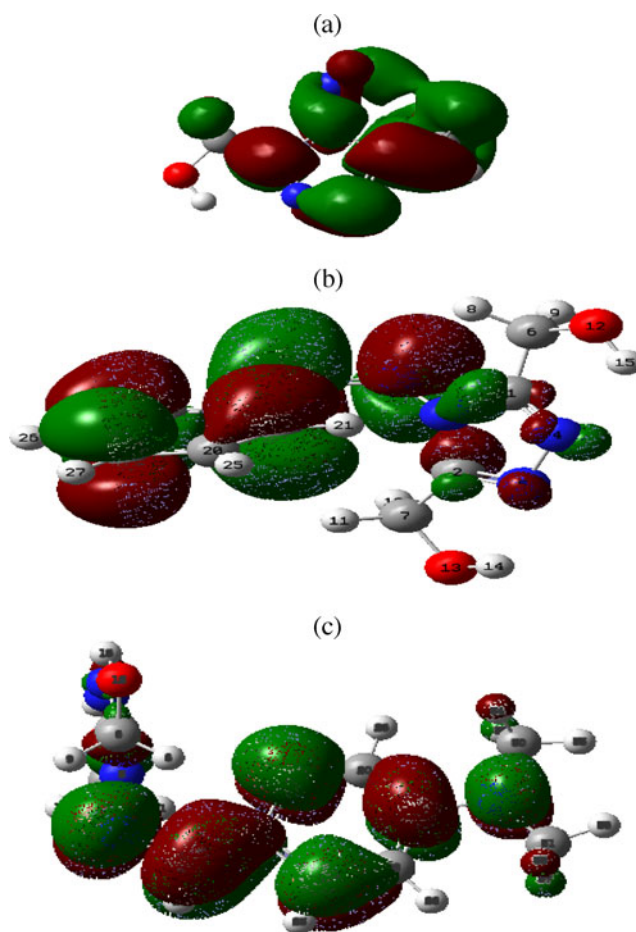**Figure 5.** Highest occupied molecular orbital (HOMO) of inhibitors: (**a**) ATD, (**b**) BATD and (**c**) DBATD.

Figure 6. Lowest unoccupied molecular orbital (LUMO) of inhibitors: (**a**) ATD, (**b**) BATD and (**c**) DBATD.

Table 3. Calculated quantum chemical properties for triazole derivatives ATD, BATD and DBATD.

Molecule	Total energy (eV)	HOMO (eV)	LUMO (eV)	ΔE(eV)	μ	I	A	χ	η	ΔN
ATD	−14330	−0·1382	−6·9805	6·8423	4·9367	0·1382	6·9805	3·5500	−3·4212	0·0467
BATD	−21653	−2·4035	−6·9190	4·5155	7·1341	2·4035	6·9190	4·6612	−2·2577	0·3169
DBATD	−25299	−1·7910	−5·9402	4·1491	9·5912	1·7910	5·9402	3·8656	−2·0745	0·1532

Table 4. Condensed Fukui functions for case when the molecule receives charge from metal surface.

	ATD			BATD			DBATD	
Atoms	f_k^+	f_k^-	Atoms	f_k^+	f_k^-	Atoms	f_k^+	f_k^-
C(1)	0·0268	0·2664	C(1)	0·1639	0·0103	C(1)	0·0068	0·0012
C(2)	0·0265	0·2675	C(2)	0·1596	0·0113	C(2)	0·0061	0·0012
N(3)	0·2039	0·2025	N(3)	0·0035	0·0039	N(3)	0·0043	0·0082
N(4)	0·4807	0·0425	N(4)	0·1308	0·0062	N(4)	0·0160	0·0039
N(7)	0·1181	0·0524	N(5)	0·1529	0·0040	N(5)	0·0176	0·0043
N(8)	0·1186	0·0531	C(6)	0·0302	0·0020	C(6)	0·0009	0·0011
C(9)	0·0009	0·0122	C(7)	0·0218	0·0011	C(7)	0·0007	0·0018
O(12)	0·0533	0·0006	O(12)	0·1166	0	O(12)	0·0012	0·0004
C(14)	0·0009	0·0123	O(13)	0·0662	0·0002	O(13)	0·0011	0·0002
O(17)	0·0053	0·0006	N(16)	0·0014	0·2204	N(16)	0·1685	0·3837
			C(17)	0·0001	0·0798	C(17)	0·3106	0·0895
			C(18)	0·0001	0·1160	C(18)	0·0128	0·2310
			C(19)	0·0001	0·0898	C(19)	0·0154	0·1624
			C(20)	0	0·0091	C(20)	0·2054	0·0061
			C(22)	0·0001	0·0226	C(22)	0·2202	0·0115
			C(24)	0	0·1630	C(24)	0·0855	0·2558
			C(28)	0·0003	0·2564	C(27)	0·0102	0·4791
						N(29)	0·5524	0·0920
						C(30)	0·0108	0·0025
						C(31)	0·0102	0·0025
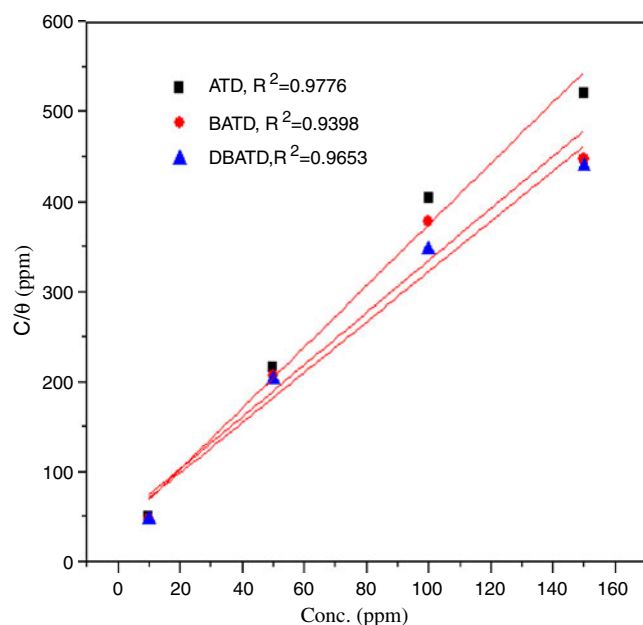
Figure 7. Langmuir's isotherm for adsorption of triazole derivatives in 1 M HNO$_3$ on copper surface at 298 K.

The values of surface coverage (θ), corresponding to different concentrations of inhibitors at 298 K have been used to get best linearity isotherm (Bouklah *et al* 2006). The adsorption isotherms generally considered were:

Temkin isotherm, $\exp f(\theta) = K_{ads}C$,

Langmuir isotherm, $\dfrac{\theta}{1 - \theta} = K_{ads}C$,

Frumkin isotherm, $\dfrac{\theta}{1 - \theta}\exp - 2f(\theta) = K_{ads}C$,

Freundlich isotherm, $\theta = K_{ads}C$,

where K_{ads} is the equilibrium constant of the inhibitor adsorption process, C the inhibitor concentration and f the factor of energetic in homogeneity, the values of surface coverage (θ) can be obtained from impedance measurements according to the equation

$$\theta = \frac{R_{ct} - R_{ct}^*}{R_{ct}}.$$

The Langmuir isotherm was found to provide the best description of the adsorption behaviour. Plots of C/θ vs C

yield a straight line as shown in figure 7. In both cases the linear regression coefficients (R^2) are almost equal to 1, indicating that the adsorption of ATD, BATD and DBATD obeys the Langmuir adsorption isotherm and K_{ads} values can be calculated from the intercepts of the straight lines on the C/θ-axis, the K_{ads} is related to the standard free energy of adsorption, ΔG^0_{ads} with the following equation:

$$\Delta G^0_{ads} = -RT \ln (55 \cdot 5 K_{ads}), \qquad (11)$$

the value 55·5 in the above equation is the molar concentration of water in solution in mol/l (John *et al* 2010a). Thermodynamic parameters for adsorption process obtained from Langmuir adsorption isotherm for the inhibitors are given in table 5. The negative value of ΔG^0_{ads} obtained on the addition of inhibitors indicate that adsorption of ATD, BATD and DBATD is spontaneous in nature (Flis and Zakroczymski 1996). It is generally accepted that the value of ΔG^0_{ads} up to -20 kJ mol^{-1} indicates physisorption, the electrostatic interactions between charged molecules and charged metal, while the value around -40 kJ mol^{-1} or smaller indicate typical chemisorptions, the charge sharing or charge transfer from the inhibitor molecules to the metal surface to form a covalent bond (Bentiss *et al* 2005; John *et al* 2010b). The values of ΔG^0_{ads} in this measurement range from -22 to -37 kJ mol^{-1} (table 5) which suggest that the adsorption of
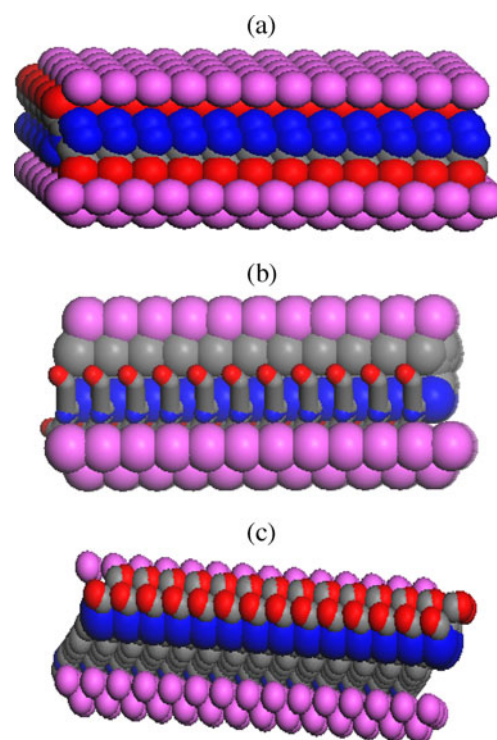

Figure 8. Modes of adsorption of (**a**) ATD, (**b**) BATD and (**c**) DBATD on Al (110) surface.

ATD, BATD and DBATD involves two types of interactions: chemisorption and physisorption.

3.6 *Molecular simulation study*

Molecular modeling studies provide a strong evidence for the molecular attraction of ATD, BATD and DBATD to the metal surface. The prediction of the inhibitor–surface interaction through the modeling studies lead to optimal molecular binding on the metal surface (Xia *et al* 2008; Khaled and Amin 2009).

In Monte Carlo simulation, molecular dynamics were performed on a system comprising inhibitors and aluminium (110) surface. Through Monte Carlo simulation process one can arrive at the conclusion that which out of the studied inhibitors have lowest energy. The outputs and descriptors calculated by Monte Carlo simulation are presented in table 6. The parameters presented in table 6 include total energy of the substrate–adsorbate configuration. The total

Table 5. Equilibrium constant and standard free energy for aluminium in 1N HNO$_3$ in presence of different concentrations of inhibitors.

Compound	Conc.	K_{ads}	$-\Delta G_{ads}$ (kJ mol^{-1})
ATD	10	2785	29·8024
	50	1885	29·8292
	100	169	22·8244
	150	1475	28·2180
	200	1171	27·6424
BATD	10	15046	34·0091
	50	3758	30·5490
	100	3977	30·6906
	150	2823	29·8361
	200	49614	36·9850
DBATD	10	19955	34·7133
	50	46216	36·8081
	100	4938	31·2307
	150	3678	30·4959
	200	67949	37·6943

Table 6. Outputs and descriptors calculated by Monte Carlo simulation for adsorption of ATD, BATD and DBATD on Al (110) surface.

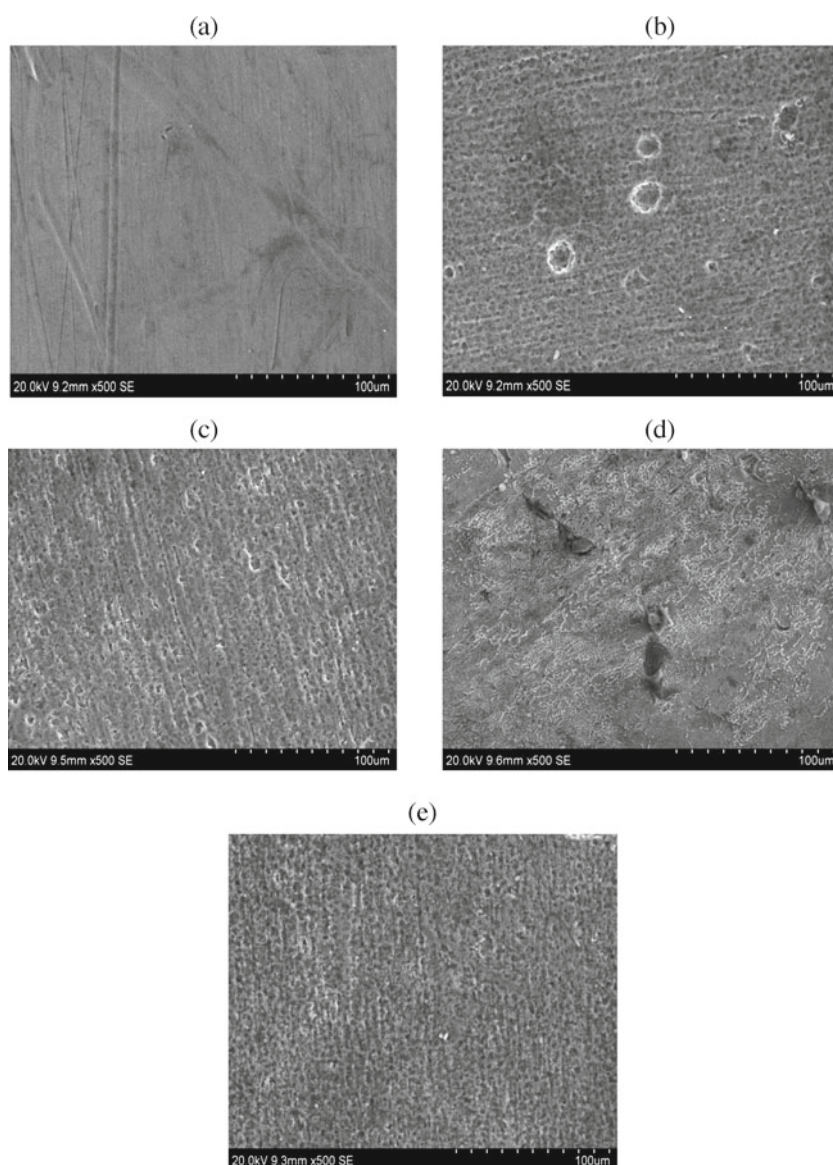| Inhibitor	Total energy (kJ mol^{-1})	Adsorption energy (kJ mol^{-1})	Rigid ad. energy (kJ mol^{-1})	Deformation energy (kJ mol^{-1})	Atomistic: dE_{ad}/dN_i	Calculated binding energy (kJ mol^{-1})
ATD	10·32	$-45782 \cdot 71$	25·32	$-45808 \cdot 04$	$-45782 \cdot 72$	45511·59
BATD	704·26	$-63182 \cdot 44$	565·17	$-63786 \cdot 97$	$-63221 \cdot 79$	63390·72
DBATD	1518·72	$-73655 \cdot 20$	1003·85	$-74659 \cdot 09$	$-73655 \cdot 24$	73629·31

Figure 9. SEM images of (**a**) aluminium metal, (**b**) in 1N HNO$_3$ without inhibitor, (**c**) in presence of 200 ppm of ATD after 24 h, (**d**) in presence of 200 ppm of BATD after 24 h and (**e**) in presence of 200 ppm of DBATD after 24 h weight loss measurements.

energy is defined as the sum of the energies of the adsorbate components, rigid adsorption energy and deformation energy. In this study, the substrate energy is taken as zero.

The adsorption energy is defined as the sum of the rigid adsorption energy and deformation energy for the adsorbate components. The rigid adsorption energy reports the energy, in kcal mol^{-1}, released (or required) when the unrelaxed adsorbate components are adsorbed on the substrate. The deformation energy reports the energy released when the adsorbed adsorbate components are relaxed on the substrate surface. dE_a/dN_i which defines the energy of substrate–adsorbate configurations where one of the adsorbate components has been removed. As can be seen from

table 6, DBATD has maximum total energy and rigid adsorption energy which is in conformity with the experimental results. The close contact between the inhibitor molecules and Al(110) surface as well as the best adsorption configuration for the studied compounds are shown in figure 8.

3.7 *Scanning electron microscopy*

Surface examination using SEM was carried out to study the effect of inhibitors on the surface morphology of aluminium metal. Figure 9(a) shows SEM image of a polished aluminium sample. Figure 9(b) shows SEM image of

aluminium surface after immersion in 1N HNO$_3$ solution with no additives for 24 h. This micrograph reveals that the surface was strongly damaged in the absence of inhibitor. Figures 9(c), (d) and (e) show SEM images of the surface of aluminium immersed for 24 h in 1N HNO$_3$ solution containing 200 ppm of the inhibitor molecules. The faceting observed in figures 9(c), (d) and (e) was gone and the surface was free from pits and it was smooth. It can be concluded that the rate of corrosion is less in the presence of inhibitors. Magnification of SEM images clearly shows that more polished surface is formed in the case of DBATD (Wang *et al* 2002; Babic-Samardzija *et al* 2005; Zhao *et al* 2005; Ramesh and Adhikari 2009). These observations also support the results of electrochemical studies and quantum chemical calculations pertaining to these inhibitors.

4. Conclusions

(I) The inhibitor molecules show good inhibitive efficiency for aluminium in aerated 1N HNO$_3$.

(II) The percentage inhibition efficiency increases with increase in concentration of ATD, BATD and DBATD and decreases with longer exposure periods at 298 K.

(III) Higher surface coverage on the metal surface was obtained in 1N HNO$_3$ solution with higher inhibitor concentrations.

(IV) Results of polarization studies suggest that the inhibitors, ATD, BATD and DBATD, act as mixed type inhibitors.

(V) The inhibitor molecules adsorb on the metal surface and blocking the reaction sites. The surface area available for attack of the corrosive species decreases with increasing inhibitor concentrations.

(VI) Molecular dynamics simulations are performed to investigate the adsorption behaviour of ATD, BATD and DBATD on aluminium surface.

(VII) The relationship between efficiency of inhibition of aluminium corrosion in 1N HNO$_3$ by ATD, BATD and DBATD and the E_{HOMO}, E_{LUMO}, $E_{LUMO}-E_{HOMO}$ and ΔN were calculated by DFT method.

(VIII) The results of quantum chemical calculations and electroanalytical studies are in conformity with each other and the inhibitor molecule DBATD acts as better inhibitor than BATD and ATD.

Acknowledgements

References

Abd El-Maksoud S A 2002 *Corros. Sci.* **44** 803

Agrawal R and Namboodhiri T K G 1990 *Corros. Sci.* **30** 37

Ailor W H 1971 *Handbook of corrosion testing and evaluation* (New York: John Wiley and Sons)

Ajmal M, Mideen A S and Quraishi M A 1994 *Corros. Sci.* **36** 79

Amin M A and Khaled K F 2010 *Corros. Sci.* **52** 1194

Amin M A, Abed El-Rehim S S, El-Sherbini E E F and Bayyomi R S 2007 *Electrochim. Acta* **52** 3588

Arslan T, Kandemirli F, Ebenso E E, Love I and Alemu H 2009 *Corros. Sci.* **51** 35

Ashassi-Sorkhabi H, Ghalebsaz-Jeddi N, Hashemzadeh F and Jahani H 2006 *Electrochim. Acta* **51** 3848

Babic-Samardzija K, Lupu C, Hackerman N and Barron A R 2005 *J. Mater. Chem.* **15** 1908

Bag S K, Chakraborty S B and Chaudhari S R 1993 *J. Indian Chem. Soc.* **70** 24

Bentiss F, Traisnel M and Lagrene M 2000 *Corros. Sci.* **42** 127

Bentiss F, Lebrini M and Lagrene M 2005 *Corros. Sci.* **47** 2915

Bouklah M, Hammouti B, Lagrene M and Bentiss F 2006 *Corros. Sci.* **48** 2831

Chetouani A, Hammouti B, Benhadda T and Daoudi M 2005 *Appl. Surf. Sci.* **249** 375

Dessai M N, Dessai M B, Shah C B and Dessai S M 1986 *Corros. Sci.* **26** 827

Do D 1980 *Adsorption analysis in equilibria and kinetics* (London: Imperial College Press)

Ebenso E E, Arslan T, Kandemirli F, Caner N and Love I 2010 *Int. J. Quantum Chem.* **110** 1003

Flis J and Zakroczymski T 1996 *J. Electrochem. Soc.* **143** 2458

Frisch M J *et al* 2003 *Gaussian 03* (Pittsburgh: Gaussian Inc.)

Gece G 2008 *Corros. Sci.* **50** 2981

John S, Joseph B, Aravindakshan K K and Joseph A 2010a *Mater. Chem. Phys.* **122** 374

John S, Joseph B, Balakrishnan K V, Aravindakshan K K and Joseph A 2010b *Mater. Chem. Phys.* **123** 218

Jones D A 1983 *Principles and prevention of corrosion* (NJ: Prentice Hall) 2nd ed.

Khaled K F and Al-Qahtani M M 2009 *Mater. Chem. Phys.* **113** 150

Khaled K F and Amin M A 2009 *Corros. Sci.* **51** 1964

Khaled K F, Fadl-Allah S A and Hammouti B 2009 *Mater. Chem. Phys.* **117** 148

Klingele M H, Moubaraki B, Murray K S and Brooker S 2005 *Chem. Eur. J.* **11** 692

Labjar N, Lebrini M, Bentiss F, Chihib N E, Hajjaji S E and Jama C 2010 *Mater. Chem. Phys.* **119** 330

McCafferty E 2005 *Corros. Sci.* **47** 3202

McCafferty E, Pravadic V and Zettlemoyer A C 1999 *Trans. Faraday Soc.* **66** 237

Pearson R G 1963 *J. Am. Chem. Soc.* **85** 3533

Pearson R G 1988 *Inorg. Chem.* **27** 734

Pourbaix M 1966 *Atlas of electrochemical equilibria in aqueous solutions* (New York: Pergamon Press)

Quartarone G, Battilana M, Bonaldo L and Tortato T 2008 *Corros. Sci.* **50** 3467

Ramesh S V and Adhikari A V 2009 *Mater. Chem. Phys.* **115** 618

Sastri V S and Perumareddi J R 1997 *Corros. Sci.* **53** 617

Solmaz R, Kardas G, Culha M, Yazici B and Erbil M 2008 *Electrochim. Acta* **53** 5941

Talati J D and Modi R M 1975 *Br. Corros. J.* **10** 103

Tsuru T, Haruyama S and Gijutsu B 1978 *J. Jpn. Soc. Corros. Eng.* **27** 573

Wang H L, Fan H B and Zheng J S 2002 *Mater. Chem. Phys.* **77** 655

Wang H, Wang X, Wang H, Wang L and Liu A 2007 *J. Mol. Model* **13** 147

Xia S, Qiu M, Yu L, Liu F and Zhao H 2008 *Corros. Sci.* **50** 2021

Yang W and Mortier W J 1986 *J. Am. Chem. Soc.* **108** 5708

Zhang Q B and Hua Y X 2010 *Mater. Chem. Phys.* **119** 57

Zhao P, Liang Q and Li Y 2005 *Appl. Surf. Sci.* **252** 1596